

# Highly Stretchable, Ultra-Soft, and Fast Self-Healable Conductive Hydrogels Based on Polyaniline Nanoparticles for Sensitive Flexible Sensors

Xiaohui Yu, Haopeng Zhang, Yufei Wang, Xiaoshan Fan,\* Zibiao Li, Xu Zhang,\* and Tianxi Liu\*

Herein, novel conductive composite hydrogels are developed with high stretchability, ultra-softness, excellent conductivity, and good self-healing ability. The hydrogels are formed in the water/glycerol binary solvent system, in which the polyaniline nanoparticles (PANI-NPs) are incorporated into the poly(poly(ethylene glycol) methacrylate-co-acrylic acid) (P(PEG-co-AA)) scaffolds via the dynamically electrostatic interactions and hydrogen bonds. The PANI-NPs serve as conductive fillers to assign conductivity to the hydrogel, while the enhanced interfacial interactions between the PANI-NPs and P(PEG-co-AA) matrix endow the hydrogel with high stretchability (>1000%), low modulus ( $\approx 6$  kPa), excellent elasticity ( $\eta = 0.07$ , energy loss coefficient at 500% strain), and fast self-healing ability (93.3% after 10 mins). Particularly, the desirable anti-freezing property is achieved by introducing a binary solvent system. The composite hydrogel-based sensors are proposed, with the states-independent properties, low detection limit (0.5% strain and 25 Pa), highly linear dependence, and excellent anti-fatigue performance (>1000 cycles). In addition, during the practical wearable sensing tests, various external stimulus and human motions can be detected, including speaking, writing, joint movement, or even small water droplets, indicating the potential applications for the next generation of epidermal sensors.

## 1. Introduction

Flexible wearable sensors have shown a variety of promising applications in the emerging fields like soft robotics, health monitoring, and artificial intelligence.<sup>[1]</sup> They are able to mimic the complex functions of human skin by transducing external stimuli such as pressure, temperature, humidity, and other physiological parameters into detectable electronic signals.<sup>[2]</sup> To fully mimic the properties of skin, it is necessary to develop advanced skin-like materials with low elastic modulus, high stretchability, and good self-healing capability.<sup>[3]</sup> Among them, hydrogels, a kind of typical soft materials, have been widely utilized to fabricate intelligent sensors because of their tissue-like softness and biocompatibility.<sup>[4]</sup> In addition, the human skin also has other important functional features such as the repeated self-healing ability, good electrical conductivity, and ultrahigh sensitivity.<sup>[5]</sup> These unique features could make human skin to autonomously and repeat-

edly self-repair after mechanical damages and sense subtle environmental variations.<sup>[4a,6]</sup> However, it still remains a major challenge to design the hydrogels engaging such multiple functions mentioned above.

Conductive hydrogels combining the features of hydrogels with electrical conductivity have been emerging as promising materials to design flexible sensors.<sup>[7]</sup> Up to now, a number of conductive hydrogels have been fabricated by introducing electrical conductors into the polymer networks.<sup>[8]</sup> Generally, the used electrical conductors can be mainly classified into two types, namely, ionic (such as salt and ionic liquids) and electronic conductors (e.g., conducting polymers, carbon and metallic nanomaterials).<sup>[7a]</sup> Comparatively, the electronic conductive hydrogels possess ultrahigh sensitivities to force and strain, low detection limit, and excellent conductivity.<sup>[9]</sup> However, the electrical conductive hydrogels always display low stretchability (<200%), large hysteresis loop, and poor mechanical strength due to the weak interfacial interactions between the polymer scaffolds and rigid fillers.<sup>[10]</sup> Moreover, the rapid deterioration occurs in the conductivity because of the aggregation and/or break of the integrated conductive fillers during the

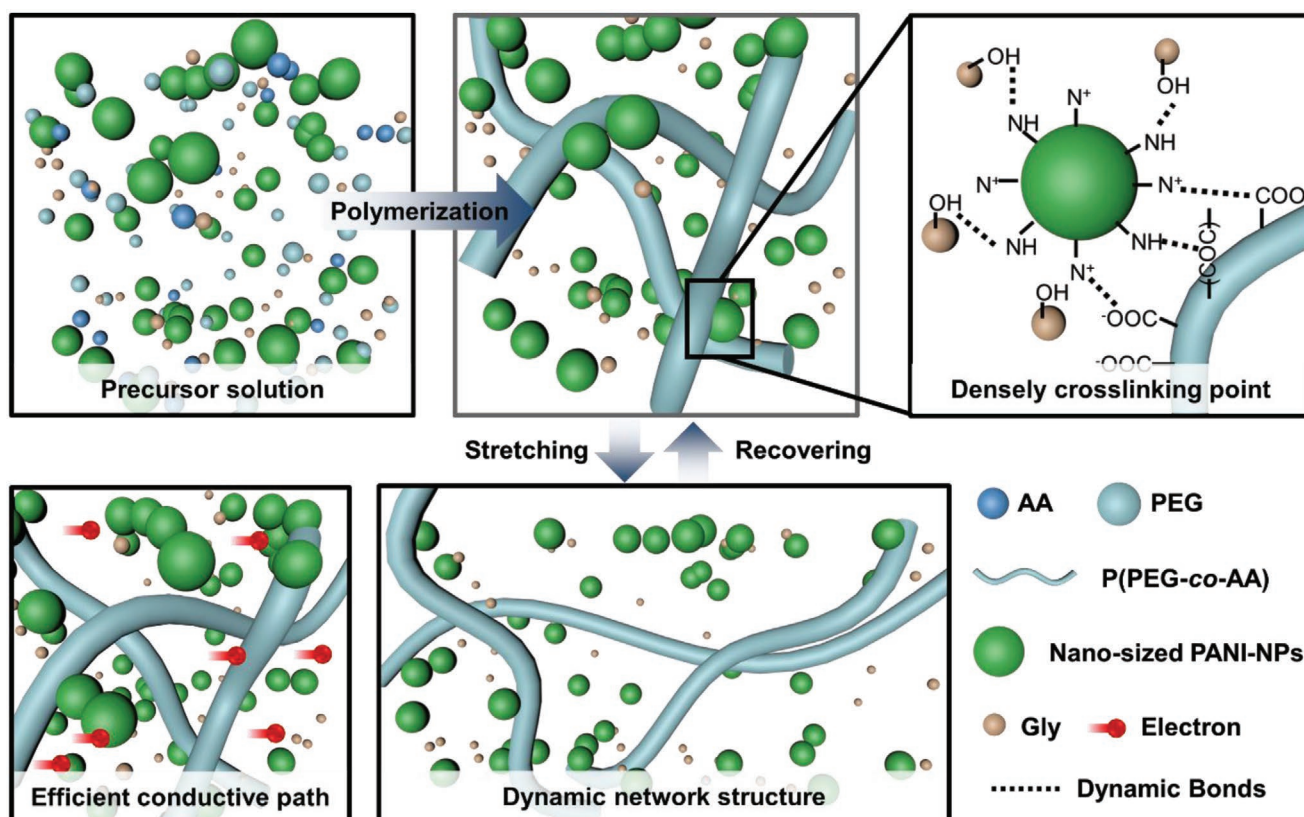
X. Yu, H. Zhang, Y. Wang, X. Fan, T. Liu  
State Key Laboratory for Modification of Chemical Fibers and Polymer Materials  
College of Materials Science and Engineering  
Donghua University  
Shanghai 201620, P. R. China  
E-mail: xsfan@dhu.edu.cn

Z. Li  
Institute of Sustainability for Chemicals, Energy and Environment (ISCE2)  
A\*STAR (Agency for Science, Technology and Research)  
Singapore 138634, Singapore

X. Zhang, T. Liu  
Key Laboratory of Synthetic and Biological Colloids  
Ministry of Education  
School of Chemical and Material Engineering  
International Joint Research Laboratory for Nano Energy Composites  
Jiangnan University  
Wuxi, Jiangsu 214122, P. R. China  
E-mail: xuzhang@jiangnan.edu.cn; txliu@jiangnan.edu.cn

 The ORCID identification number(s) for the author(s) of this article can be found under <https://doi.org/10.1002/adfm.202204366>.

DOI: 10.1002/adfm.202204366



**Scheme 1.** Schematic illustration of the dynamic cross-linked networks by introducing the nano-sized PANI-NPs hybrid hydrogels (nPHHs).

cyclic deformation process for practical use.<sup>[11]</sup> These shortcomings limit their applications for detecting the large-scale strain and long-term conductive stability. So, how to strengthen the interfacial interactions between the conductive fillers and the polymer matrix is pivotal for enhancing the physical properties of the conductive hydrogels and ensuring no occurrence in conductive damages during the repeated deformation process.<sup>[12]</sup> Although various design strategies and fabrication methods have been proposed to enable the conductive hydrogels with improved interfacial interactions, most of them are carried out with a tedious and low efficiency procedure.<sup>[13]</sup> Meanwhile, few of the reported conductive hydrogels meet the unique combination of skin-like properties.

Here, we reported a facile yet simple strategy for the fabrication of the novel conductive glycerol-water hydrogels featuring with the unique nano-sized PANI-NPs serving as the conductive fillers and cross-linkers. The schematic structure of the poly [poly (ethylene glycol) methacrylate-co-acrylic acid (AA)] [P(PEG-co-AA)]/PANI hybrid hydrogels (nPHHs) was depicted in **Scheme 1**, in which the networks are closely associated via multi noncovalent interactions including hydrogen-bonding and electrostatic interactions. The glycerol-water hydrogels were obtained by the elaborately designed polymerization process of PEG and AA in the presence of PANI-NPs. The P(PEG-co-AA) were used as the biocompatible flexible networks to readily form the electrostatic interactions and hydrogen bonds with the PANI-NPs, thus significantly improving the interfacial interactions between the conductive fillers and polymer matrix. It

is worth noting that the traditional PANI is brittle and stiff, and the poor strength/flexibility inevitably causes the damage of the conductive networks during the stretching process. As compared, the as-formed PANI-NPs, prepared via a multiphase synthesis technique, can withstand the large strain and stress due to their unique structures. Most importantly, the PANI-NPs could be reversibly rearranged with the polymer chains during the stretching-releasing process to form the complete conductive paths, thus imparting the sensors with stable and reproducible sensing performance. The as-prepared PANI-based hydrogels simultaneously exhibit the high stretchability, ultra-softness, high elasticity, self-healing, and anti-freezing properties, which could be considered as the promising materials for the assembly of high-performance flexible sensors.

## 2. Results and Discussion

### 2.1. Preparation and Characterizations

The overall synthetic process began with the multiphase reaction to obtain the nano-sized PANI-NPs as schematically illustrated in **Figure 1a**. In a typical synthesis process, the solution containing the mixture of aniline monomer, Gly, and phytic acid (PA) was mixed with the aqueous solution dissolved with the ammonium persulfate (APS) as the oxidative reagent. Among them, the PA molecules not only play the role of the acid dopants to increase the electrical conductivity but also offer

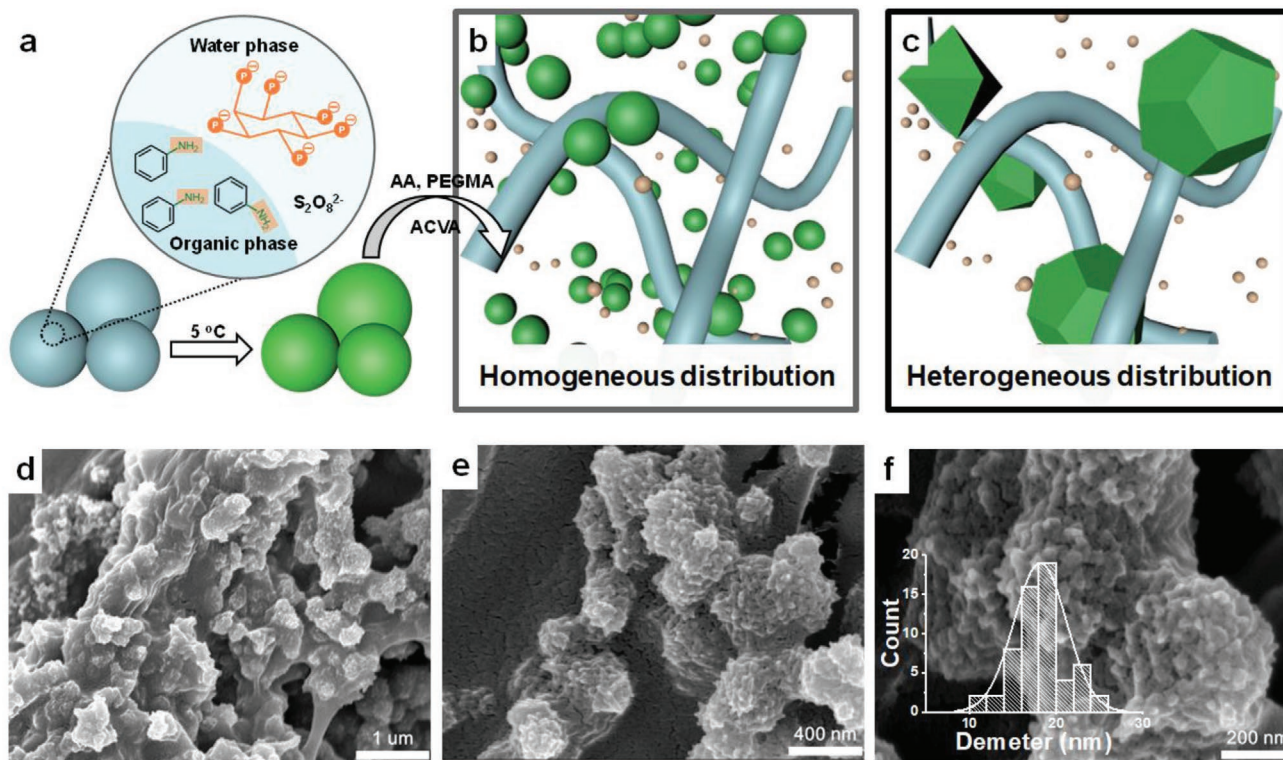


**Figure 1.** Schematic illustration of a) the multiphase reaction mechanism, b) the hydrogel networks with homogeneous distributed nano-sized PANI-NPs in the nPHHs, and c) the heterogeneous distributed PANI particles in the ordinary PHHs. d–f) Scanning electron microscopy (SEM) images of the nPHH-3. The inset in (f) represents the diameter distribution of the PANI-NPs.

the additional physical dynamic cross-linking points to construct a part of the multiple dynamic cross-linking networks.<sup>[7b]</sup> Because of the phase separation between the organic and aqueous phase, the emulsion could be obtained, which could be confirmed by the Tyndall effect scattering experiment (Figure S1, Supporting Information). With the polymerization of the nano-sized PANI-NPs, the homogeneous dark-green (the color of the PANI) solution was obtained after uninterrupted vigorous stirring for 24 h at  $-5\text{ }^{\circ}\text{C}$  (Figure S2, Supporting Information). As followed, the PEG and AA monomers, and the initiator (4,4'-azobis(4-cyanovaleric acid) (ACVA)) were added to form the homogeneous precursor solution. Finally, the nPHHs were successfully prepared through the convenient free radical polymerization process at  $70\text{ }^{\circ}\text{C}$  for over 5 h. The hybrid hydrogels were denoted as nPHH-1, nPHH-2, and nPHH-3, as the initial aniline concentration was 0.5, 1.0, and 1.5 wt.%, respectively. Meanwhile, the control samples (i.e., PANI hybrid hydrogels) were denoted as PHHs, which were fabricated in the single-solvent of water, while the other conditions of preparation were as same as the nPHH-3.

Benefiting from the sufficient intermolecular interactions, the nano-sized PANI-NPs were homogeneously dispersed in the polymer matrix, as schematically illustrated in Figure 1b. However, in the ordinary PHHs, the rigid polymeric chains of PANI would lead to the inadequate dispersibility, resulting in the obvious aggregations in the hydrogel matrix (Figure 1c; Figure S3, Supporting Information). As shown in Figure 1d, the nPHHs exhibit the porous structures, similar to the ordinary

hydrogels. Differently, in the present work, the nano-sized PANI-NPs were tightly attached to the porous polymer skeletons uniformly (Figure 1e,f). The data of the size of the PANI-NPs could be obtained from the SEM images and analyzed by the software of ImageJ. After the analysis, the size and distribution of the PANI-NPs was shown in the inset of Figure 1f. The average size of the PANI-NPs was  $\approx 18.17\text{ nm}$ , and the median size was  $\approx 18.35\text{ nm}$ , showing a highly normal distribution. The well-dispersed PANI-NPs were capable of constructing the continuous conductive networks to endow the hydrogels with excellent conductivity because of the special  $\pi$ -conjugated polymeric chains. As shown in Figure S4 (Supporting Information), the hydrogels could serve as the conductor to light on the LED bulb. Moreover, the conductivity of the nPHHs increases obviously as the PANI-NPs content increases (Figure S5, Supporting Information), where the nPHH-3 exhibit the highest electronic conductivity ( $74.32\text{ mS cm}^{-1}$ ), which is higher than lots of the conductive polymer-based hydrogels reported before. The electrical conductivity properties of the conductive hydrogels were further demonstrated by the electrochemical impedance spectroscopy. The Nyquist plots of the different samples were shown in Figure S6 (Supporting Information). The equivalent resistance (ER, the intersection points on the real axis) of the nPHHs decreases as the content of PANI-NPs increases. Since the specific applications for human motion sensing, the Nyquist plots of the nPHH-3 at different deformation conditions were shown in Figure S7 (Supporting Information) to reveal the conductivity stability of the hybrid hydrogels. Even

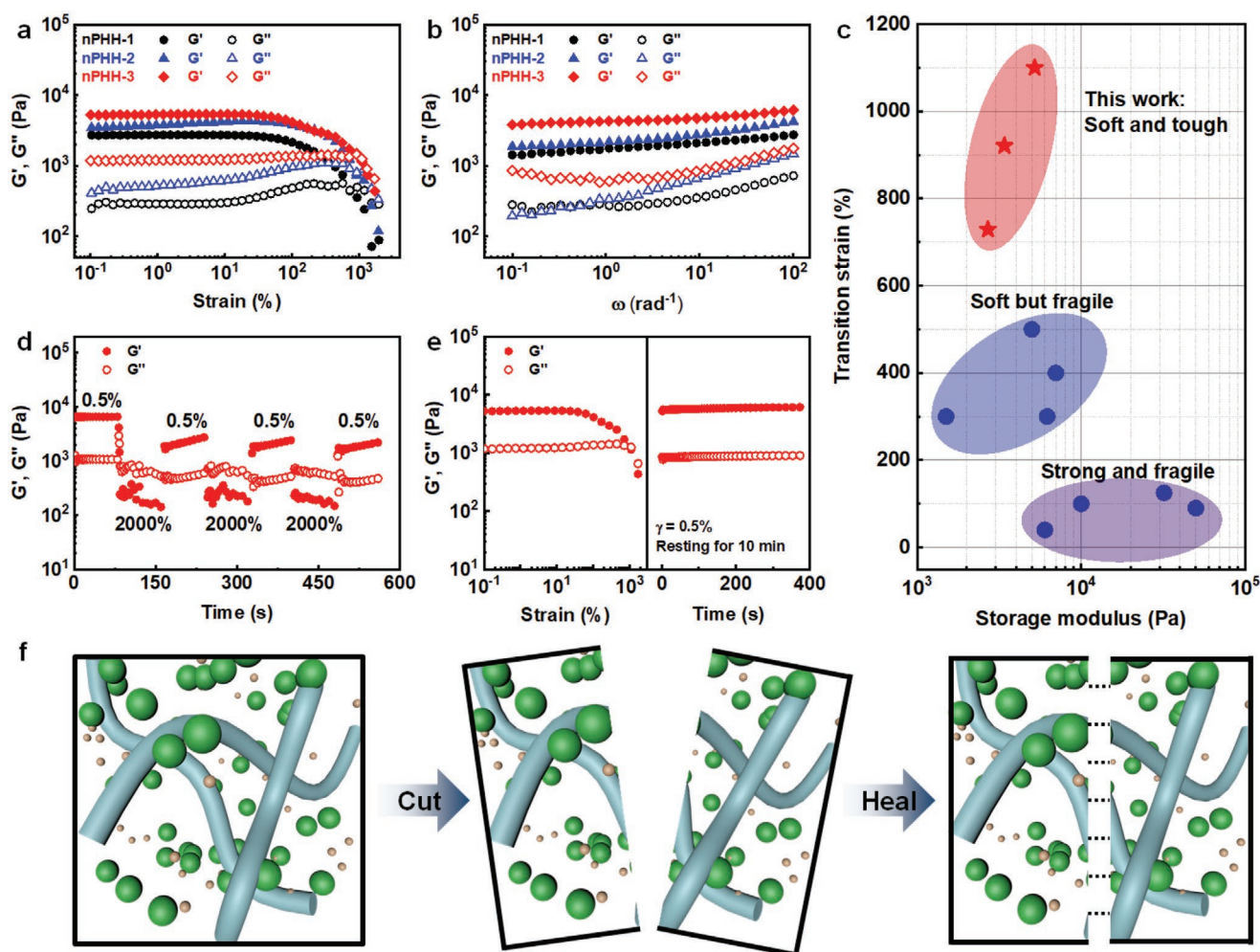


**Figure 2.** a) Rheological strain and b) angular frequency sweeping measurements of the nPHHs. c) Comparison of the storage modulus and transition strain between the nPHHs and the other conductive polymer composite hydrogels reported previously. d) Cyclic shearing strain and e) dynamic alternating strain-time sweeping measurements of the nPHH-3. f) Schematic illustration of the super-fast self-healing mechanism of the nPHHs during the cutting-healing process.

though the ER of the nPHH-3 has changed during the deformation process, the calculated conductivity changes slightly.

## 2.2. Intrinsic Dynamic Characteristics

The dynamic mechanical measurements were also conducted to reveal the intrinsic viscoelastic of the nPHHs. At the small strain range, the nPHHs exhibit the gel-like state, where the storage modulus ( $G'$ ) is higher than the loss modulus ( $G''$ ) (Figure 2a), confirming that the hydrogel networks of the nPHHs were conserved adequately. As the shearing strain increases, the transition points could be observed, which correspond to the signals of the rupture of the hydrogel networks. Meanwhile, with increasing the nano-sized PANI content, the nPHH-3 show the highest modulus ( $\approx 5000$  Pa) and transition strain ( $\approx 1000\%$ ), indicating the strengthening effect of the nano-sized PANI-NPs. In the frequency sweeping measurements, all the samples show the excellent ductility and ultra-low modulus ( $<10\ 000$  Pa) over the entire

frequency range (Figure 2b). The super soft and flexible performance of the as-prepared nPHHs were totally different from the ordinary rigid conductive polymer hybrid hydrogels reported previously (Figure 2c),<sup>[10b,11,14]</sup> and were of great significance for the development of the epidemic sensors. Based on the reviews, the modulus of human skin is much lower than the ordinary conductive polymeric hydrogels. As a result, those ordinary hydrogel-based sensors with high mechanical performance were difficult to make the coincident deformations with the epidermis/skin under micro-strain, resulting in the poor detective sensitivity. Thus, the super-soft performance of nPHHs is beneficial in improving the sensing sensitivity and realizing the low detection limit of the flexible sensors.<sup>[6,15]</sup>

Besides, the oscillatory rheology measurements were conducted to investigate the recoverability of the dynamic networks of the nPHH-3. As the hydrogels were subjected to the shearing strain at 0.5%, the  $G'$  maintains at  $\approx 5000$  Pa and always higher than the  $G''$  ( $\approx 1000$  Pa), indicating the nPHH-3 remain solid-like elastic network (Figure 2d). After that, the  $G'$

and  $G''$  would intersect as the amplitude oscillatory shear turns up to 2000%, indicating the breakdown of the hydrogel networks. Subsequently, the  $G'$  immediately exceeds the  $G''$  with the healing efficiency of  $\approx 40\%$ , once the shearing strain turns back to the previous value of 0.5%, proving the excellent instantaneously self-healing performance of the dynamic networks of the nPHH-3. In the next cycles, the nPHH-3 exhibit the recyclable self-healing performance. To further investigate the self-healing efficiency of the nPHH-3, the dynamic alternating strain-time sweeping tests were further conducted as presented in Figure 2e. When the healing time only lasts 10 min, the  $G'$  recovers to the primary value adequately, with the healing efficiency of  $\approx 100\%$  (Figure 2e). This super-fast self-healing performance is responsible for the efficiently dissociation and reformation of the dynamic cross-linked networks, as schematically illustrated in Figure 2f.

### 2.3. Environmental Stability

The excellent anti-freezing, anti-heating, and long-term stability properties were further realized by the incorporation of Gly, which was the well-known anti-freezing agent and nonionic kosmotrope.<sup>[16]</sup> At first, the nPHHs exhibit the excellent anti-freezing properties (Figure 3a). Under the subzero temperature,

the strong hydrogen bonds would be formed between the Gly and the water molecules, disrupting the formation of the ice crystalline. When the water was the only solvent, the PHHs were frozen into the glass state and lost the flexibility of storage at  $-30\text{ }^\circ\text{C}$  for 24 h (Figure 3b). The sharp peak at  $4.5\text{ }^\circ\text{C}$  corresponding to the freezing point in the differential scanning calorimetry (DSC) curve also confirmed the poor freezing resistance of the PHHs (Figure 3c). Differently, the nPHHs still exhibit the elastic state (Figure 3a), which could be twisted at the extremely low temperature, without any obvious peak in the DSC curve (Figure 3c). Also, the introduction of Gly could lower the vapor pressure of the system, leading to the excellent high temperature resistance.<sup>[17]</sup> When the PHHs were stored under  $60\text{ }^\circ\text{C}$  for 24 h, they would be dried out and became hard polymers with irregularly shrink, and thus would no longer exhibit the elasticity. In contrast, the nPHHs could be still moist and maintain the gel state, which also keeps highly conductive and mechanical performance under such extreme environment. Under the low temperature ( $-20\text{ }^\circ\text{C}$ ), the LED bulb could be successfully lighted in the nPHH-based circuit, while the PHHs did not work (Figure S8, Supporting Information). The temperature sweeping rheology measurements were conducted to investigate the mechanical anti-fatigue performance of the nPHHs at different temperatures. In the wide temperature range from 5 to  $75\text{ }^\circ\text{C}$ , the nPHHs always show the gel

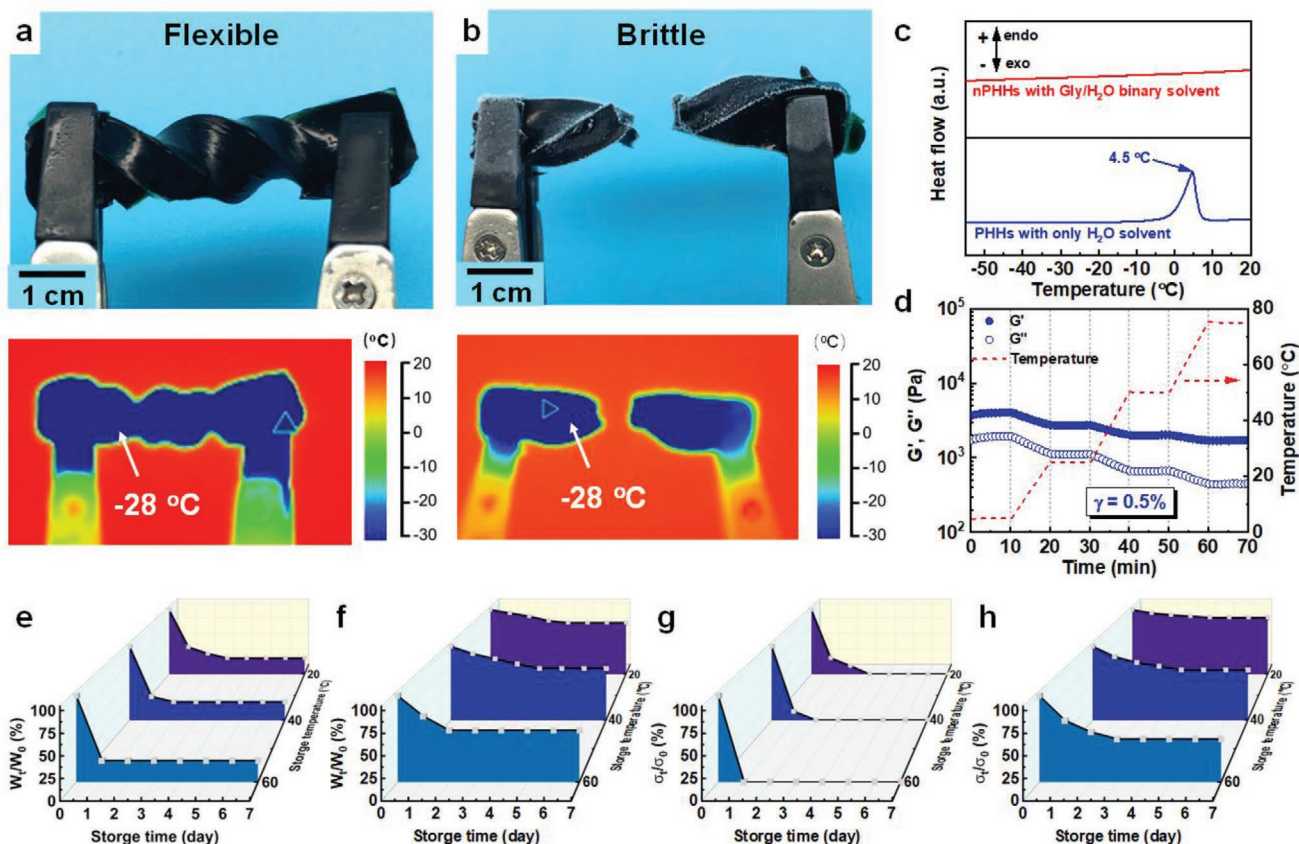


**Figure 3.** Digital and infrared images of the a) nPHHs and b) PHHs twisted after being stored at  $-30\text{ }^\circ\text{C}$  for 24 h. c) DSC measurements of the nPHHs and PHHs. d) Temperature sweeping measurements of the nPHHs at different temperatures. Weight change of the e) PHHs and f) nPHHs in different storage time and temperatures. Conductivity stability of the g) PHHs and h) nPHHs in different storage time and temperatures.

state with no significant decrease in modulus in the long-term usage (Figure 3d).

The long-term stability of the nPHHs could be certified by the fact that there is no performance degradation after the long storage time at different conditions. To address the evidence, the weight of the PHHs and the nPHHs were measured at different storage time. Blaming on the water evaporation in the hydrogels, the weight of the PHHs lost to only  $\approx 20\%$  of the original state after 3 days in the normal condition ( $20\text{ }^\circ\text{C}$ ), and finally transformed into the dried polymer state (Figure 3e). Meanwhile, the evaporation rate was positively correlated with the temperature. As the storage temperature increases up to  $60\text{ }^\circ\text{C}$ , the weight of the PHHs dropped quickly, close to the water content, after the initial 2 days. In contrast, the weight of the nPHHs did not have obvious drift ( $<20\%$ ) in different conditions during the long storage time (Figure 3f), which could be attributed to the effective prevention of the water evaporation

due to the strong interactions between the Gly and the water molecules. At the same time, the conductivity of the nPHHs was also stable without marked change (Figure 3h), which was superior to the PHHs (Figure 3g), confirming that the electrical percolation paths are relatively stable inside of the nPHHs.

## 2.4. Mechanical Properties

Due to the existence of the multiple reversible cross-linked networks, the nPHHs would exhibit the unique dynamic mechanical characteristic properties. The stress–strain curves of the nPHHs with various contents of the nano-sized PANI-NPs were shown in Figure 4a. Benefiting from the strong interactions between the PANI-NPs and the polymer matrix, as the nano-sized PANI content increases, the mechanical strength is obviously enhanced from 21.4 to 25.9 kPa, while the frac-

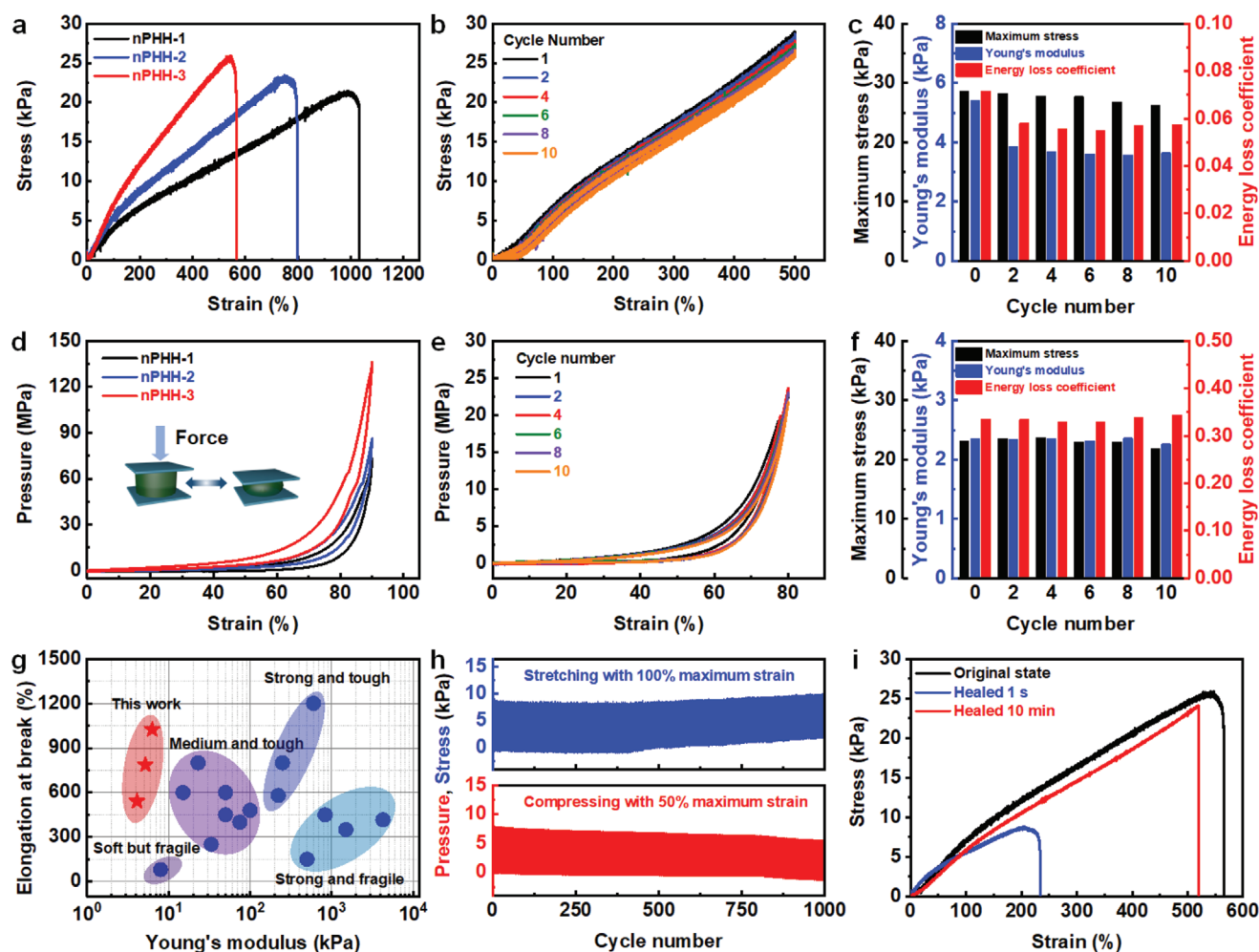


**Figure 4.** a) Stress–strain curves of the nPHHs with different contents of the nano-sized PANI-NPs. b) Ten cyclic tensile curves of the nPHH-3 at the maximum strain of 500%. c) Maximum stress, Young's modulus, and the energy loss coefficient of the nPHH-3 in the cyclic tests. d) Pressure–strain curves of the nPHHs at the maximum compressive strain of 90%. e) Ten cyclic compressive curves under 80% strain of the nPHH-3. f) Maximum pressure, compressive Young's modulus, and energy loss coefficient of the nPHH-3 in the cyclic compressing tests. g) Comparison of the modulus and elongation at break between the as-prepared nPHHs and the other conductive polymer composite hydrogels. h) Consecutive 1000 cycles loading–unloading tests under 100% stretching and 50% compressive strain. i) Tensile curves of the nPHH-3 at the original state and healed state with different healing time.

ture strain decreases from 1030% to 580%. The tensile cyclic tests were conducted to reveal the energy dissipation mechanism, where the maximum stress, Young's modulus, dissipated energy ( $\Delta U$ ), and energy loss coefficient ( $\eta$ ) were considered.<sup>[18]</sup> The dissipated energy ( $\Delta U$ ) was defined as the area of the hysteresis loop of the loading–unloading curve, corresponding to the rupture of the dynamic networks, and the energy loss coefficient ( $\eta$ ) represents the efficient of the energy dissipation. Figure S9 (Supporting Information) shows the first two laps stress–strain curves under the maximum strain of 100%. The nPHH-3 exhibit the best self-recovery performance, while the maximum stress maintains at  $\approx 92\%$ , compared with the first cycle, owing to the most abundant dynamic bonds in the networks. In the wide strain range from 100% to 500%, the inconspicuous hysteresis loops could be observed from every loading–unloading cycle, demonstrating the excellent edacity of the hydrogels (Figures S10 and S11, Supporting Information). The consecutive tensile curves at the tremendous strain of 500% were then presented in Figure 4b. Nearly the same Young's modulus, maximum stress, and  $\eta$  could be observed at different cycles, which were summarized in Figure 4c, indicating the excellent elasticity of the nPHH-3. The remarkable dynamic property could be contributed to the reversible destruction and reassociation of the multiple dynamic noncovalent cross-linked networks.

The compressive tests were further performed to evaluate the mechanical deformation tolerant ability and elasticity of the nPHHs. As shown in Figure 4d, the nPHHs could tolerate the extremely compressive deformation of 90%, which is totally different from the normal PANI hybrid hydrogels. With the increase in the nano-sized PANI-NPs content, the maximum compressive stress gradually increases from 70.7 to 135.8 kPa. The stability of the nPHHs under the extremely compressive deformation of 80% was also investigated. During the ten uninterrupted loading–unloading cycles, the nPHHs show the almost constant mechanical performance (Figure 4e). At the first cycle, the  $\eta$  of the nPHH-3 was only 0.34, indicating a little damage of the hydrogel networks. Except the first cycle, the value decreases slightly and stabilizes at  $\approx 0.33$  after ten cycles, confirming the excellent elasticity of the hydrogels. The maximum stress remains stable in the cyclic tests and maintains  $\approx 94.3\%$  (i.e., 21.8 kPa) in the end (Figure 4f). The super soft and deformation tolerant performance of the nPHHs is completely different from the intrinsic rigidity of the ordinary conductive polymer composite hydrogels reported previously (Figure 4g).<sup>[7b,10b,11,14a-c,19]</sup>

To further investigate the anti-fatigue performance of the nPHHs, the continuous stretching (100% strain) and compressing (50% strain) loading–unloading tests were performed (Figure 4h). During the cyclic tests, the mechanical performance keeps highly stable, demonstrating the excellent elasticity and anti-fatigue properties, where the abundant dynamic bonds in the polymer matrix could endow the nPHHs with the superior self-healing performance. The tensile tests of the healed samples in different healing time were also performed to investigate the healing efficiency of the nPHHs (Figure 4i). Surprisingly, the elongation at break ratio and maximum stress of the healed nPHH-3 with the healing time of only 1 s would respectively recover to 41.2% (i.e., 233.9%) and 33.87% (i.e., 8.7 kPa) of

the original sample, indicating the excellent instant self-healing performance. As the healing time prolongs to 10 min, the fracture strain and maximum stress could respectively be highly restored to 92.2% (i.e., 518.4%) and 93.3% (i.e., 23.9 kPa) of the sample before cutting.

## 2.5. Sensing Performance

With a sandwich structured design, the super-soft elastic conductive hydrogels were assembled into the sensitive deformable sensors for future human-motion interface monitoring, as illustrated in Figure 5a. Figure 5b shows the resistance–strain curves of the assembled sensors during the stretching–releasing tests in the maximum strain of 200%. As shown in Figure S12 (Supporting Information), the gauge factor ( $GF$ ) of the nPHH-based sensor was calculated. At the strain range of 0–50%, the  $GF$  is 1.46. In the higher strain range (50–200%), the  $GF$  zooms to 2.43, ensuring the good sensing ability of the nPHH-based flexible sensors, which might be comparable to the previously-reported works (see Table S1, Supporting Information),<sup>[20]</sup> confirming the good detection sensitivity. Besides, a mass of reported hydrogel-based sensors always show the large hysteresis loop during the long-term usage. Their relative resistance changes not only rely on the external strain but also on the deformation state (stretching or releasing). In other words, for a given stress, the resistance in the stretching state ( $R_s$ ) is not equal to the value in the releasing state ( $R_r$ ).<sup>[18b]</sup> On the contrary, the nPHH-based sensors exhibit the intriguing states-independent properties, that is,  $R_s = R_r$  toward to the strain of 200%. It can be seen that the electronic signal curves exhibit no hysteresis loop during the loading–unloading process, which was important for the real-time acquisition of the resistance data. With increasing the applied maximum strain (50%, 100%, 150%, and 200%), the relative resistance ( $\Delta R/R_0$ ) of the nPHH-based flexible sensors increases and the signals always keep stable and repeatable (Figure 5c). It is worth mentioned that the ultralow deformation (0.5%, 1.0%, 1.5%, and 2.0%) could also been detected sensitively as shown in Figure 5d. Benefiting from the excellent conductivity of the nPHHs, the response time of the nPHH-based flexible sensors during the stretching–recovering process was only 140 ms (Figure 5e).

Besides, the nPHH-based flexible sensors could also exhibit the excellent long-term service stability thanks to the excellent dynamic performance of the hybrid hydrogels. To investigate the tensile frequency tolerance of the sensor devices, a series of stretching–releasing tests at various stretching rates were then performed under 50% maximum strain. As shown in Figure S13 (Supporting Information), the relative resistance exhibits the negligible changes during the stretching–releasing process at 50, 100, and 200 mm min<sup>-1</sup> deformation rate. Shown in Figure 5f is the electronic patterns of the sensors undergoing the cyclic cutting and self-healing process, where the baselines of the resistive signals are stable and completely repeatable during the cutting–healing process. Meanwhile, the electrical healing time was 140 ms in the first and second cutting–healing process, which was comparable to the reported work, indicating the outstanding self-repairable electrical properties of the nPHHs.<sup>[21]</sup> As compared with the reported works, the nPHHs

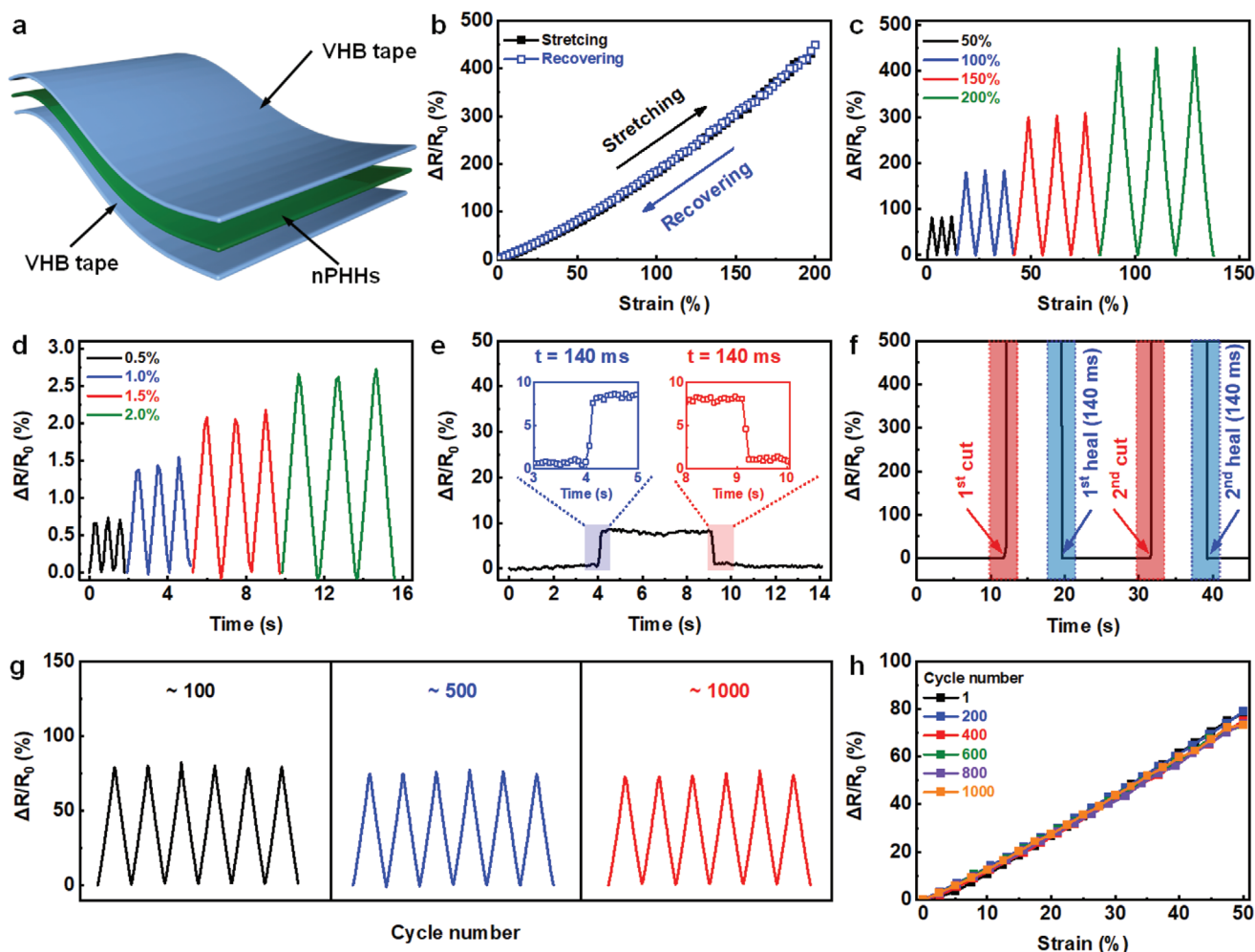


**Figure 5.** a) Schematic illustration of the multilayered structure of the nPHH-based flexible sensors. b) Relative resistance ( $\Delta R/R_0$ ) variations of the sensors with 200% maximum strain during the stretching and recovering process.  $\Delta R/R_0$  of the sensors during four loading-unloading cycles with c) high (50%, 100%, 150%, and 200%) and d) low (0.5%, 1.0%, 1.5%, and 2.0%) maximum strain. e) Response time during the stretching and recovering process. f) Self-healing performance tests of the sensors. g) The 1000 stretching cycles at 50% maximum strain. h) Resistance-strain curves of the sensors in 1, 200, 400, 600, 800, and 1000 cycles.

not only possess the important performance of self-healing but also exhibit the high sensitivity (Table S1, Supporting Information).<sup>[22]</sup> Owing to the tensile stability of the nPHHs, the sensors also own the excellent cyclic fatigue resistance. After 1000 uninterrupted cycles, the sensing performance of the sensors still remains stable (Figure 5g). Most importantly, the resistance-strain curves are always highly linear with a high degree of coincidence, as drawn in Figure 5h.

The nano-sized PANI-NPs were employed in the present work to construct the efficient conductive paths in the nPHHs, which could also result in the excellent mechanical-electronic response performance. The resistance-pressure curve of the nPHH-based flexible sensors (as schematically illustrated in Figure 6a) shows linearly as the pressure ranges from 0 to 1 kPa with a high sensitivity ( $S = 0.18 \text{ kPa}^{-1}$ ) (Figure 6b), attributing to the excellent elastic and super softness of the nPHHs. Meanwhile, the as-prepared nPHH-based flexible sensors possess the reproducible and stable resistance-pressure curve over the range of pressure detection from 200 to 1000 Pa (Figure 6c).

As shown in Figure 6d, the resistance variations of the sensors under 500 Pa pressure still maintains stability as the compressive rate increases from 100 to 200  $\text{mm min}^{-1}$ , suggesting the excellent frequency tolerance. Different from the normal conductive polymer-based pressure sensors, the nPHH-based sensors have the higher detection accuracy. In addition, the nPHH-based sensor devices could also sense the small pressure from 100 to 500 Pa step-wisely, as demonstrated in Figure 6e. The most important thing is that the nPHH-based sensors exhibit the immediate response to the extreme small pressure (25 Pa, equal to the pressure generated by a mass of 250 mg on one square centimeter) during the loading-unloading process, as shown in Figure 6f, with the response time shorter than 240 ms.

Thanks to the remarkable sensing performance, the nPHH-based flexible devices could be applied for the future soft robotic applications. As presented in Figure 7a, the sensors could serve as the flexible tablets to detect the different English letters of “D”, “H”, and “U”, where the output electronic

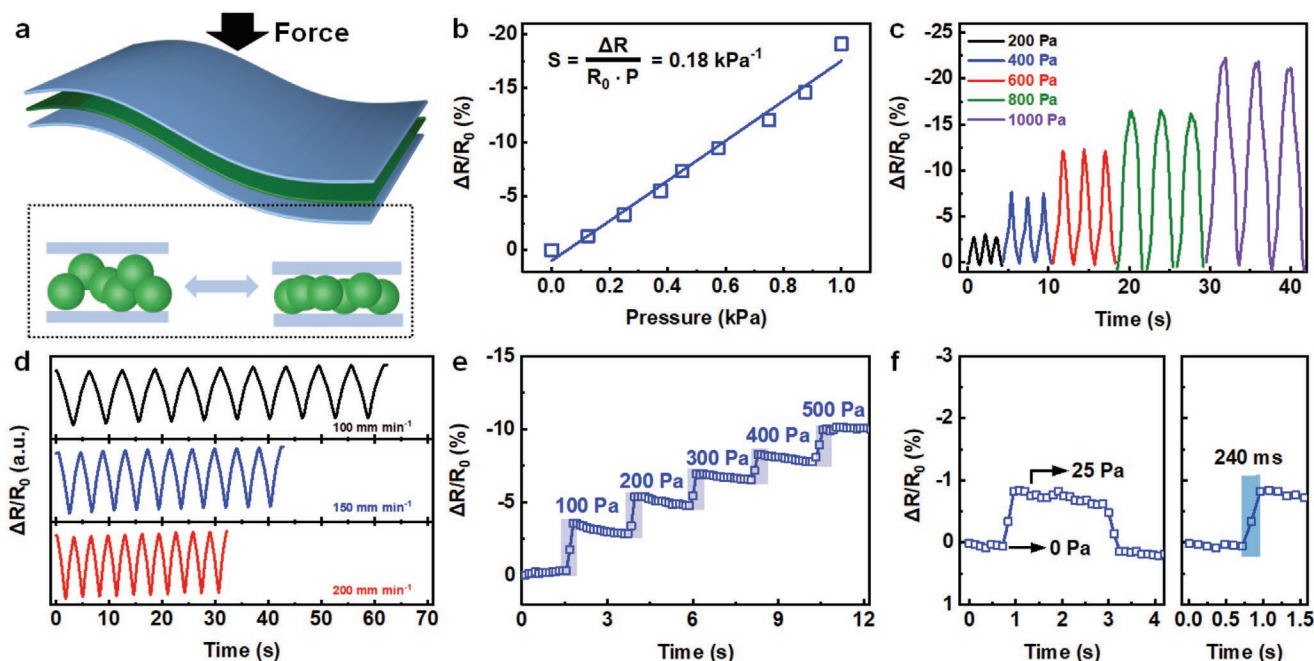


**Figure 6.** a) Schematic of the highly sensitive electronic-mechanical response mechanism. b)  $\Delta R/R_0$  of the nPHH-based sensors c) under 0–1 kPa pressure and d) during three loading–unloading cycles as the pressure ranges from 200 to 1000 Pa. d) Frequency fatigue performance, e) stepwise resistance–pressure pattern as the pressure ranges from 0 to 500 Pa at 100 Pa per step, and f) instant response of the nPHH-based pressure sensors.

signals were mainly determined by the pressure amplitude and writing speed. Besides, the sensors could attach onto the fingers to monitor the bending angles. As the angles increase from  $0^\circ$  to  $90^\circ$ , the  $\Delta R/R_0$  increases rapidly. In the recovering process, when the bending angle reduces from  $90^\circ$  to  $0^\circ$ ,

the resistance continuously decreases and eventually return back to the original state (Figure 7b). Moreover, the rapid and accurate resistance changes could also be obtained from the nPHH-based sensors during the bending of wrist and elbow, as illustrated in Figure 7c. In addition, the extremely light body

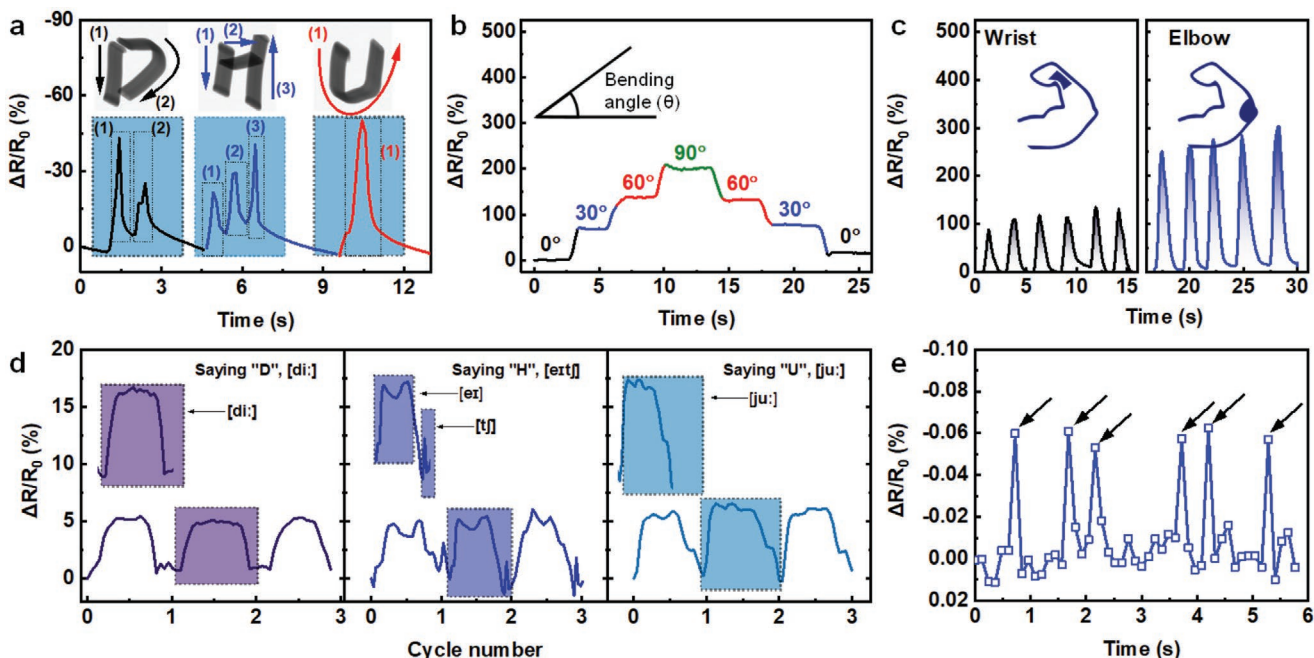


**Figure 7.** a) Signature sensing patterns when writing different English letters on the nPHH-based sensor devices. The relative resistance changes of the attached sensor devices when b) bending the fingers, c) moving the wrist and elbow, d) and speaking different English letters. e) Real-time relative resistance changes when the water droplets land on the nPHH-based sensors.

movements and weak external stimulus could also be detected. After being attached onto the laryngeal of the volunteer, the different phonations could be recognized by the nPHH-based sensors. As shown in Figure 7d, the different electronic patterns correspond to the different words of “D”, “H”, and “U”. Notably, the nPHH-based sensors could even detect the rain drop (mimicked by using the small water droplets falling from 20 cm height) (Figure 7e). Therefore, the as-prepared super soft and elastic hydrogel (nPHH) based sensors would have great potentials in the epidermal sensing area.

### 3. Conclusions

In summary, a novel strategy was designed and developed to fabricate high-performance conductive hydrogels by using glycerol/water mixture as the binary solvent. The nano-sized PANI-NPs, instead of the traditional PANI nanofibers, were incorporated into the hydrogels as conductive fillers, which not only empower the good conductivity to the hydrogels but also reinforce the hydrogel networks. The synergetic effect of the dynamic hydrogen-bonding and electrostatic interactions between PANI-NPs and P(PEG-co-AA) networks account for the impressive stretchability ( $\approx 1000\%$ ), ultra-softness ( $\approx 6$  kPa), and high self-healing efficiency (93.3%) at room temperature, which are super to the common conducting polymer-based hydrogels. Due to the inhibited ice crystallization by the introduction of glycerol, the as-prepared hydrogels (nPHHs) can maintain the high stretchability under very low temperature ( $-28$  °C). Besides, the hydrogel-based sensors could possess the combination of the low detection limit, highly linear dependence, and excellent anti-fatigue performance. On basis of these good performance, the nPHH-based flexible sensors could differentiate the signature of writing and detect various human motions and external stimulus including joint movement, speaking, or even small water droplets, exhibiting the promising practical applications in the field of wearable devices.

### 4. Experimental Section

**Materials:** The acrylic acid (AA, 99%), poly (ethylene glycol) methacrylate (PEG, Mw  $\approx 360$ , 98%), phytic acid solution (PA, 50% in H<sub>2</sub>O), aniline (ANI, 99.8%), ammonium persulfate (APS, 98%), 4,4'-azobis(4-cyanovaleic Acid) (ACVA, 98%), and glycerol (Gly, 98%) were all purchased from Shanghai Aladdin Co.

**Preparation of nPHHs:** The preparation of the nPHHs followed a convenient one-pot and two-step method. At first, the nano-sized PANI-NPs solution was prepared, following the multiphase reaction mechanism. Solution A was prepared by dissolving 500  $\mu$ L ANI and 1 mL PA solution in 15 mL Gly. The 0.5 g mass of APS was dissolved in 15 mL water, serving as the oxidative reagent. These two solutions were then quickly mixed together and kept stirring vigorously at the low temperature (0 °C) to form a homogeneous solution. Upon the polymerization of ANI into PANI, the well dispersed dark-green solution was obtained after 24 h. Subsequently, the monomers (5 mL AA and 5 mL PEG) and initiator ACVA (1 g) was added into the above solution. The obtained precursor solution was transferred into the PTFE mold and polymerized at the temperature of 70 °C for 5 h.

**Mechanical Measurements of nPHHs:** The mechanical properties of the nPHHs were measured by the universal tester (SUNS UTM2000)

at room temperature. For tensile measurements, strip-shaped hydrogel samples ( $20 \times 10 \times 2$  mm<sup>3</sup>) were stretched at the stretching rate of 50 mm min<sup>-1</sup>. For compression tests, the cylinder-shaped samples (5 mm in diameter and 10 mm in height) were placed on the lower plate compressed by the upper plate, and the compressive speed was 10 mm min<sup>-1</sup>. The dissipated energy ( $\Delta U$ ) was defined as the area of hysteresis loop encompassed by the loading-unloading curve, calculated by the following formula:

$$\Delta U = \int_{\text{loading}} \sigma d\varepsilon - \int_{\text{unloading}} \sigma d\varepsilon \quad (1)$$

where  $\sigma$  was the stress,  $\varepsilon$  was the strain. the energy loss coefficient ( $\eta$ ) represented the efficient of the energy dissipation.

$$\eta = \frac{\Delta U}{U} \quad (2)$$

$$U = \int_0^{\sigma_{\max}} \sigma d\varepsilon \quad (3)$$

where  $U$  is the elastic energy stored in the materials when it is loaded elastically to a stress  $\sigma_{\max}$  in the cycle.

### Supporting Information

Supporting Information is available from the Wiley Online Library or from the author.

### Acknowledgements

This work was financially supported by the National Natural Science Foundation of China (52103074 and 21875033), the Natural Science Foundation of Shanghai (21ZR1402800), the Innovation Program of Shanghai Municipal Education Commission (2021-01-07-00-03-E00108), and the China Postdoctoral Science Foundation (2021M690597).

### Conflict of Interest

The authors declare no conflict of interest.

### Data Availability Statement

Research data are not shared.

### Keywords

conductive hydrogels, flexible sensors, highly stretchable, polyaniline nanoparticles, self-healable, ultra-soft

Received: April 18, 2022

Revised: May 14, 2022

Published online: June 1, 2022

[1] a) Q. Zheng, J.-h. Lee, X. Shen, X. Chen, J.-K. Kim, *Mater. Today* **2020**, *36*, 158; b) S.-T. Han, H. Peng, Q. Sun, S. Venkatesh, K.-S. Chung, S. C. Lau, Y. Zhou, V. A. L. Roy, *Adv. Mater.* **2017**, *29*,

- 1700375; c) M. Gong, L. Zhang, P. Wan, *Prog. Polym. Sci.* **2020**, *107*, 101279.
- [2] a) *Nat. Nanotechnol.* **2017**, *12*, 1017; b) Y. Qiao, Y. Wang, H. Tian, M. Li, J. Jian, Y. Wei, Y. Tian, D.-Y. Wang, Y. Pang, X. Geng, X. Wang, Y. Zhao, H. Wang, N. Deng, M. Jian, Y. Zhang, R. Liang, Y. Yang, T.-L. Ren, *ACS Nano* **2018**, *12*, 8839; c) Y. Wang, Y. Liu, N. Hu, P. Shi, C. Zhang, T. Liu, *Sci. China Mater.* **2022**, <https://doi.org/10.1007/s40843-021-1977-5>; d) J. Rao, Z. Chen, D. Zhao, R. Ma, W. Yi, C. Zhang, D. Liu, X. Chen, Y. Yang, X. Wang, J. Wang, Y. Yin, X. Wang, G. Yang, F. Yi, *Nano Energy* **2020**, *75*, 105073.
- [3] a) Y. Ren, Z. Liu, G. Jin, M. Yang, Y. Shao, W. Li, Y. Wu, L. Liu, F. Yan, *Adv. Mater.* **2021**, *33*, 2008486; b) M. Wang, Y. Luo, T. Wang, C. Wan, L. Pan, S. Pan, K. He, A. Neo, X. Chen, *Adv. Mater.* **2021**, *33*, 2003014; c) T. Wang, D. Qi, H. Yang, Z. Liu, M. Wang, W. R. Leow, G. Chen, J. Yu, K. He, H. Cheng, Y.-L. Wu, H. Zhang, X. Chen, *Adv. Mater.* **2019**, *31*, 1803883; d) X. Yu, Y. Wang, H. Zhang, X. Fan, T. Liu, *ACS Appl. Mater. Interfaces* **2021**, *13*, 53091; e) X. Yu, Y. Zheng, Y. Wang, H. Zhang, H. Song, Z. Li, X. Fan, T. Liu, *Chem. Mater.* **2022**, *34*, 1110.
- [4] a) X. Yu, Y. Zheng, H. Zhang, Y. Wang, X. Fan, T. Liu, *Chem. Mater.* **2021**, *33*, 6146; b) X. Li, L. He, Y. Li, M. Chao, M. Li, P. Wan, L. Zhang, *ACS Nano* **2021**, *15*, 7765; c) H. Zhou, J. Lai, B. Zheng, X. Jin, G. Zhao, H. Liu, W. Chen, A. Ma, X. Li, Y. Wu, *Adv. Funct. Mater.* **2022**, *32*, 2108423.
- [5] G. Ge, Y. Lu, X. Qu, W. Zhao, Y. Ren, W. Wang, Q. Wang, W. Huang, X. Dong, *ACS Nano* **2020**, *14*, 218.
- [6] S. Liu, R. Zheng, S. Chen, Y. Wu, H. Liu, P. Wang, Z. Deng, L. Liu, *J. Mater. Chem. C* **2018**, *6*, 4183.
- [7] a) B. W. Walker, R. Portillo Lara, E. Mogadam, C. Hsiang Yu, W. Kimball, N. Annabi, *Prog. Polym. Sci.* **2019**, *92*, 135; b) T. Wang, Y. Zhang, Q. Liu, W. Cheng, X. Wang, L. Pan, B. Xu, H. Xu, *Adv. Funct. Mater.* **2018**, *28*, 1705551.
- [8] Y. Shi, L. Peng, Y. Ding, Y. Zhao, G. Yu, *Chem. Soc. Rev.* **2015**, *44*, 6684.
- [9] a) Y. Lee, J. Myoung, S. Cho, J. Park, J. Kim, H. Lee, Y. Lee, S. Lee, C. Baig, H. Ko, *ACS Nano* **2021**, *15*, 1795; b) Z. Wang, J. Chen, Y. Cong, H. Zhang, T. Xu, L. Nie, J. Fu, *Chem. Mater.* **2018**, *30*, 8062.
- [10] a) H. Yu, P. Chen, W. Chen, Y. Liu, *Cellulose* **2014**, *21*, 1757; b) J. Han, Q. Ding, C. Mei, Q. Wu, Y. Yue, X. Xu, *Electrochim. Acta* **2019**, *318*, 660.
- [11] a) L. Li, Y. Zhang, H. Lu, Y. Wang, J. Xu, J. Zhu, C. Zhang, T. Liu, *Nat. Commun.* **2020**, *11*, 62; b) A. Khan, R. R. Kisannagar, C. Gouda, D. Gupta, H.-C. Lin, *J. Mater. Chem. A* **2020**, *8*, 19954.
- [12] a) L. Li, K. Wang, Z. Huang, C. Zhang, T. Liu, *Nano Res.* **2016**, *9*, 2938; b) R. Li, L. Xia, P. Lyu, J. Zhang, Y. Wang, B. Deng, C. Zhang, X. Liu, W. Xu, *Composites Communications* **2021**, *28*, 100948; c) F. Ke, Q. Zhang, L. Ji, Y. Zhang, C. Zhang, J. Xu, H. Wang, Y. Chen, *Composites Communications* **2021**, *27*, 100817; d) Y. Liang, Y. Xiong, J. Zheng, Z. Xie, C. Chen, L. Xu, *Composites Communications* **2021**, *27*, 100888.
- [13] S. Hu, L. Zhou, L. Tu, C. Dai, L. Fan, K. Zhang, T. Yao, J. Chen, Z. Wang, J. Xing, R. Fu, P. Yu, G. Tan, J. Du, C. Ning, *J. Mater. Chem. B* **2019**, *7*, 2389.
- [14] a) M. Song, H. Yu, J. Zhu, Z. Ouyang, S. Y. H. Abdalkarim, K. C. Tam, Y. Li, *Chem. Eng. J.* **2020**, *398*, 125547; b) M. Yue, Y. Wang, H. Guo, C. Zhang, T. Liu, *Compos. Sci. Technol.* **2022**, *220*, 109263; c) K. Ren, Y. Cheng, C. Huang, R. Chen, Z. Wang, J. Wei, *J. Mater. Chem. B* **2019**, *7*, 5704; d) J. Chen, Q. Peng, T. Thundath, H. Zeng, *Chem. Mater.* **2019**, *31*, 4553; e) M. A. Darabi, A. Khosrozadeh, R. Mbeleck, Y. Liu, Q. Chang, J. Jiang, J. Cai, Q. Wang, G. Luo, M. Xing, *Adv. Mater.* **2017**, *29*, 1700533.
- [15] Y. Ma, Y. Gao, L. Liu, X. Ren, G. Gao, *Chem. Mater.* **2020**, *32*, 8938.
- [16] L. B. Lane, *Ind. Eng. Chem.* **1925**, *17*, 924.
- [17] V. Epure, M. Griffon, E. Pollet, L. Avérous, *Carbohydr. Polym.* **2011**, *83*, 947.
- [18] a) C. Shao, H. Chang, M. Wang, F. Xu, J. Yang, *ACS Appl. Mater. Interfaces* **2017**, *9*, 28305; b) G. Zhang, S. Chen, Z. Peng, W. Shi, Z. Liu, H. Shi, K. Luo, G. Wei, H. Mo, B. Li, L. Liu, *ACS Appl. Mater. Interfaces* **2021**, *13*, 12531; c) X. Meng, Y. Qiao, C. Do, W. Bras, C. He, Y. Ke, T. P. Russell, D. Qiu, *Adv. Mater.* **2022**, *34*, 2108243.
- [19] a) J. Duan, X. Liang, J. Guo, K. Zhu, L. Zhang, *Adv. Mater.* **2016**, *28*, 8037; b) C. Hu, Y. Zhang, X. Wang, L. Xing, L. Shi, R. Ran, *ACS Appl. Mater. Interfaces* **2018**, *10*, 44000; c) J. W. Kim, H. Park, G. Lee, Y. R. Jeong, S. Y. Hong, K. Keum, J. Yoon, M. S. Kim, J. S. Ha, *Adv. Funct. Mater.* **2019**, *29*, 1905968; d) Y. Lin, H. Zhang, H. Liao, Y. Zhao, K. Li, *Chem. Eng. J.* **2019**, *367*, 139; e) Q. Rong, W. Lei, L. Chen, Y. Yin, J. Zhou, M. Liu, *Angew. Chem. International Edition* **2017**, *56*, 14159; f) H. Wei, M. Lei, P. Zhang, J. Leng, Z. Zheng, Y. Yu, *Nat. Commun.* **2021**, *12*, 2082; g) F. He, X. You, H. Gong, Y. Yang, T. Bai, W. Wang, W. Guo, X. Liu, M. Ye, *ACS Appl. Mater. Interfaces* **2020**, *12*, 6442; h) Q. Zhang, Q. Wang, G. Wang, Z. Zhang, S. Xia, G. Gao, *ACS Appl. Mater. Interfaces* **2021**, *13*, 50411; i) Y. Lu, J. Han, Q. Ding, Y. Yue, C. Xia, S. Ge, Q. Van Le, X. Dou, C. Sonne, S. S. Lam, *Cellulose* **2021**, *28*, 1469.
- [20] a) Y. Jiao, Y. Lu, K. Lu, Y. Yue, X. Xu, H. Xiao, J. Li, J. Han, *J. Colloid Interface Sci.* **2021**, *597*, 171; b) C. Zheng, K. Lu, Y. Lu, S. Zhu, Y. Yue, X. Xu, C. Mei, H. Xiao, Q. Wu, J. Han, *Carbohydr. Polym.* **2020**, *250*, 116905; c) S. Zhu, H. Sun, Y. Lu, S. Wang, Y. Yue, X. Xu, C. Mei, H. Xiao, Q. Fu, J. Han, *ACS Appl. Mater. Interfaces* **2021**, *13*, 59142; d) Y. Jiao, K. Lu, Y. Lu, Y. Yue, X. Xu, H. Xiao, J. Li, J. Han, *Cellulose* **2021**, *28*, 4295; e) Y. Lu, Y. Yue, Q. Ding, C. Mei, X. Xu, Q. Wu, H. Xiao, J. Han, *ACS Appl. Mater. Interfaces* **2021**, *13*, 50281; f) K. Xu, Y. Wang, B. Zhang, C. Zhang, T. Liu, *Composites Communications* **2021**, *24*, 100677.
- [21] J. Zhang, L. Wan, Y. Gao, X. Fang, T. Lu, L. Pan, F. Xuan, *Adv. Electron. Mater.* **2019**, *5*, 1900285.
- [22] a) Q. Ding, X. Xu, Y. Yue, C. Mei, C. Huang, S. Jiang, Q. Wu, J. Han, *ACS Appl. Mater. Interfaces* **2018**, *10*, 27987; b) J. Han, H. Wang, Y. Yue, C. Mei, J. Chen, C. Huang, Q. Wu, X. Xu, *Carbon* **2019**, *149*, 1; c) Y. Xu, Q. Feng, C. Zhang, T. Liu, *Composites Communications* **2021**, *25*, 100693.